Journal of Sound and Vibration (1997) **207**(1), 33–46

STABILITY ANALYSES OF A TIMOSHENKO SHAFT WITH DISSIMILAR LATERAL MOMENTS OF INERTIA

L.-W. Chen and W.-K. Peng

Department of Mechanical Engineering, *National Cheng Kung University*, *Tainan*, *Taiwan* 70101, *Republic of China*

(*Received* 3 *September*, 1996, *and in final form* 22 *April* 1997)

The stability of a rotating shaft with dissimilar stiffnesses is studied and the influences of the stiffness ratio and axial compressive loads are discussed. A finite element model of a Timoshenko beam is adopted to approximate the shaft, and the effects of rotatory inertia, shear deformations, gyroscopic moments and torsional rigidities are taken into account. In studying the whirl properties of such shafts, it is convenient to use rotating co-ordinates to formulate the equations of motion. The results show that with the existence of the dissimilar stiffnesses, unstable zones will occur. The critical speeds will decrease and the instability regions will enlarge if the stiffness ratio is increased. The increase of the stiffness ratio consequently makes the rotating shaft more unstable. When the axial compressive loads increase, the critical speeds decrease and the zones of instability enlarge.

1. INTRODUCTION

Rapid and accurate prediction of the dynamic characteristics of rotating shafts is an important task for engineers who deal with modern rotating machinery. Many studies have been reported for the dynamic analyses of rotating circular shafts possessing equal stiffness in all directions. A comprehensive review can be found in the publications of Dimentberg [1], Rieger and Crofoot [2], Rao [3], Vance [4] and Goodwin [5]; moreover, other authors, such as Nelson and McVaush [6], Nelson [7] and Chen and Ku [8], have also made many efforts in their studies on the dynamics of circular shafts.

A shaft with dissimilar stiffness properties is occasionally encountered in two-pole generator rotors, drills, end-mills and satellite booms. Laurenson [9] used a model analysis technique to study the free vibration analysis of a rotating rectangular beam. Bauer [10] provided results for the natural frequencies of an Euler beam rotating about its longitudinal axis. The work presented by Filipch *et al*. [11], an extension of that of Bauer [10], assumed that the cross-section of the uniform spinning beam possessed only one axis of symmetry. Leung and Fung [12], using the finite element method, analyzed the vibration of spinning Euler beams with arbitrary orientations to a rotating frame. Numerical results for these works were confined to finding the critical speeds.

In the stability analyses, Dimenberg [1], Rieger and Crofoot [2] and Rao [3] have proposed the influences of stiffness asymmetry on the stability of rotors. If a shaft has dissimilar stiffness properties in the two principal directions of the cross-section, the bending natural frequencies corresponding to each stiffness are obtained. For such a shaft, an instability region can be found between the first two transverse vibration frequencies

0022–460X/97/410033 + 14 $25.00/0/sv971111

Figure 1. The shaft subjected to an axial load.

of a rotating shaft with dissimilar stiffnesses. The same phenomenon was also pointed out in the study of a cracked shaft presented by Dimarogonas and Papodopoulos [13]. Chen and Chen [14] discussed the stability problems of a cracked shaft subjected to end loads. Kammer and Schlack [15] studied an Euler beam with non-constant spin rates. The non-constant angular velocities were expressed as the sum of steady state terms. Lee [16] completed the work of Bauer [10] and displayed the instability regions of a spinning beam with distinct end conditions.

In general, although the Euler beam model is simple and neglects the transverse shear effects, it has been applied in the analyses of dynamic stability for a shaft or beam with dissimilar stiffnesses. Recently, Jei and Lee [17] used a Rayleigh beam model, including the effects of rotary inertia and gyroscopic moment, for modal analysis of an asymmetrical rotor–bearing system. The whirl speeds and mode shapes of the uniform asymmetrical shaft were investigated. Collins *et al*. [18] proposed a technique for detecting cracks in a rotating Timoshenko shaft. The time histories and frequency spectra were compared for shafts with no crack and with a crack. For a cracked shaft, Papadopoulos and Dimarogonas [19, 20] discussed the coupling effects between the longitudinal, torsional and bending vibrations. Their method was good at detection of small cracks. As described by Lee *et al*. [21, 22], the Timoshenko shaft were used in modelling an asymmetric rotor system. From their investigation, both transient and steady state analyses were illustrated.

In this paper, the Timoshenko beam model including torsional rigidity will be applied to predict the instability regions of a rotating shaft with dissimilar stiffnesses in its two principal directions of the cross-section. To study the whirl properties of such shafts, it is convenient to formulate the equations of motion in rotating co-ordinates. This is because the shaft stiffness varies in the fixed co-ordinates at twice per revolution frequency. In addition, a finite element model is used to obtain the matrix equations of motion for a rotating shaft, and the effects of axial compressive loads on the stability of a rotating shaft are also studied.

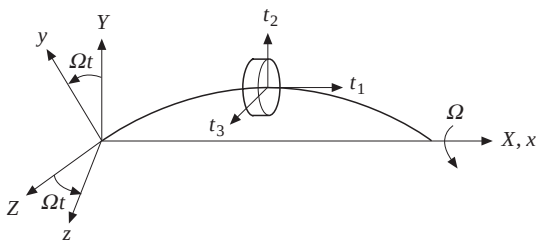

Figure 2. The reference frames of the rotating shaft.

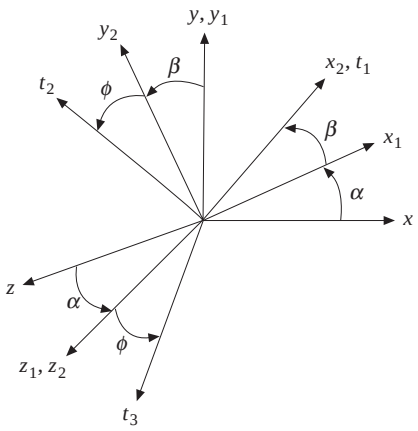

Figure 3. Three successive rotations from the rotating to the moving frame.

2. EQUATIONS OF MOTION

The dynamic stabilities of a straight rotating shaft with dissimilar lateral principal moments of inertia and subjected to axial compressive loads are investigated in the present study. Timoshenko beam theory, including rotatory inertia, shear deformations, gyroscopic moments and torsional rigidity, is applied in the formulation. The shaft with a rotating speed Ω and subjected to axial compressive loads is depicted in Figure 1. The reference frames used in the section are displayed in Figure 2. The rotating frame ($oxyz$), with unit basis vectors $\vec{i}$, $\vec{j}$ and $\vec{k}$, is obtained from the fixed frame ($OXYZ$) by a rotation of angle Ωt about the X-axis. The moving frame ($ot_1\, t_2\, t_3$), of unit basis vectors $\vec{t}_1$, $\vec{t}_2$ and $\vec{t}_3$, is attached to shaft at the centroid of a cross-section. The orientation of the moving frame ($ot_1\, t_2\, t_3$) with respect to the rotating frame ($oxyz$), using three Eulerian angles, is depicted in Figure 3. The frame ($ox_1\, y_1\, z_1$) is rotated about the y-axis by an angle α with respect to the rotating frame. Next, the $ox_2\, y_2\, z_2$ frame is rotated about the z_1-axis through an angle β with respect to $ox_1\, y_1\, z_1$. Finally, the frame ($ot_1\, t_2\, t_3$) is rotated about the x_2-axis by an angle ϕ with respect to $ox_2\ y_2\, z_2$. Hence, the orientation of the moving frame with respect to the rotating frame is

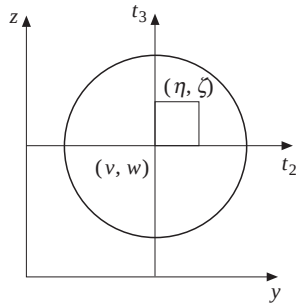

Figure 4. The translations of the centerline of the shaft.

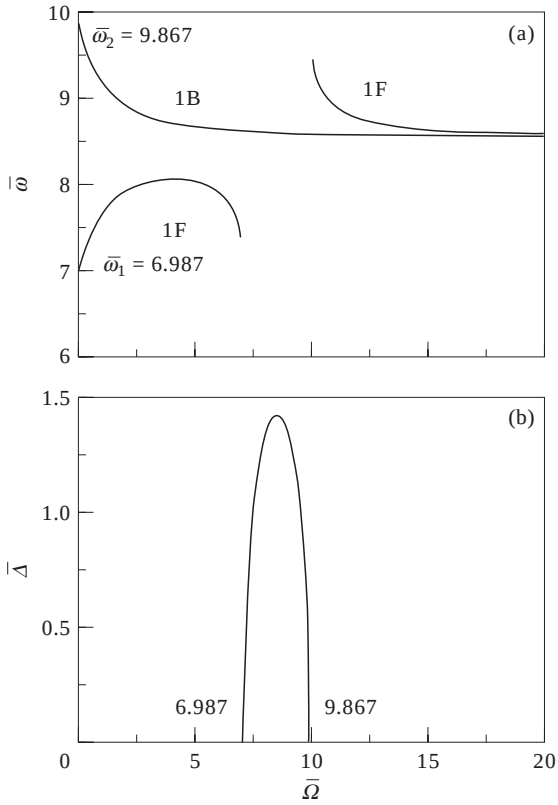

Figure 5. (a) Variation of the whirl speed parameters 1F and 1B versus the spin speed parameter; F, forward; B, backward. (b) Variation of the exponential increment parameter 1F versus the spin speed parameter.

described by

$$\begin{Bmatrix} \vec{t}_1 \\ \vec{t}_2 \\ \vec{t}_3 \end{Bmatrix} = \begin{bmatrix} 1 & 0 & 0 \\ 0 & \cos\phi & \sin\phi \\ 0 & -\sin\phi & \cos\phi \end{bmatrix} \begin{bmatrix} \cos\beta & \sin\beta & 0 \\ -\sin\beta & \cos\beta & 0 \\ 0 & 0 & 1 \end{bmatrix} \begin{bmatrix} \cos\alpha & 0 & -\sin\alpha \\ 0 & 1 & 0 \\ \sin\alpha & 0 & \cos\alpha \end{bmatrix} \begin{Bmatrix} \vec{i} \\ \vec{j} \\ \vec{k} \end{Bmatrix}. \tag{1}$$

2.1. KINETIC ENERGY

Since the stiffness of the rotating shaft is dissimilar, the kinetic energy is described in the rotating frame. The kinetic energy can be written as the sum of the translational kinetic energy of the centroidal line and the rotational kinetic energy of the cross-sections [23]. Let $\vec{r}$ be the position vector of a point on the deformed centroidal line:

$$\vec{r} = x\vec{i} + v\vec{j} + w\vec{k}. \tag{2}$$

The translational kinetic energy of the centroidal line of the shaft is

$$T_t = \tfrac{1}{2} \int_V \dot{\vec{r}} \cdot \dot{\vec{r}} \, \mathrm{d}V. \tag{3}$$

Here,

$$\dot{\vec{r}} = (\dot{v} - \Omega w)\vec{j} + (\dot{w} + \Omega v)\vec{k}. \tag{4}$$

Substituting equation (4) into equation (3) yields

$$T_t = \tfrac{1}{2}\int_0^L \rho A\{(\dot{v} - \Omega w)^2 + (\dot{w} + \Omega v)^2\}\,\mathrm{d}x. \tag{5}$$

The angular velocity of the shaft is

$$\begin{aligned}\vec{\omega} &= \Omega\vec{i} + \dot{\alpha}\vec{j} + \dot{\beta}\vec{z}_1 + \dot{\phi}\vec{t}_1\\ &= \omega_x\vec{t}_1 + \omega_y\vec{t}_2 + \omega_z\vec{t}_3,\end{aligned} \tag{6}$$

where

$$\omega_x = \Omega\cos\alpha\cos\beta + \dot{\alpha}\sin\beta + \dot{\phi},$$

$$\omega_y = \Omega\sin\alpha\sin\phi - \Omega\cos\alpha\sin\beta\cos\phi + \dot{\alpha}\cos\beta\cos\phi + \dot{\beta}\sin\phi,$$

$$\omega_z = \Omega\cos\alpha\sin\beta\sin\phi + \Omega\sin\alpha\cos\phi - \dot{\alpha}\cos\beta\sin\phi + \dot{\beta}\cos\phi.$$

Accordingly, the rotational kinetic energy is

$$T_r = \tfrac{1}{2}\int_0^L \rho\,\{I_y\,\omega_y^2 + I_z\,\omega_z^2 + J_p\,\omega_x^2\}\,\mathrm{d}x. \tag{7}$$

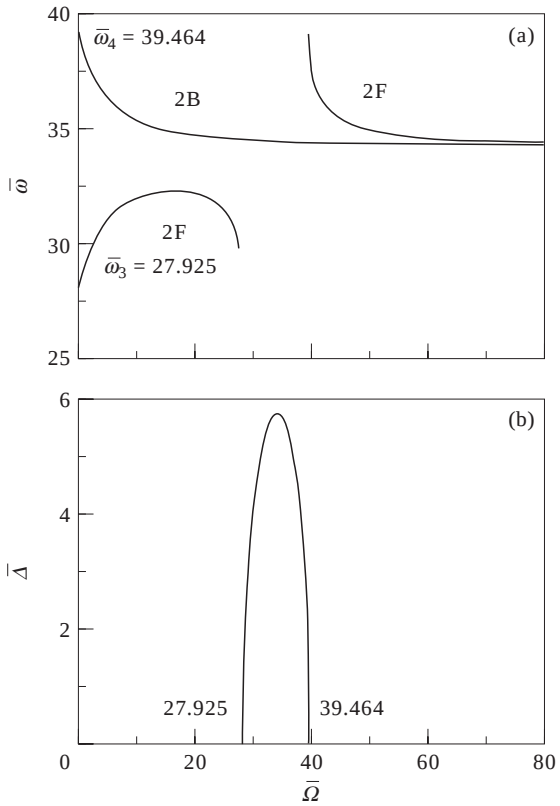

Figure 6.(a) Variation of the whirl speed parameters 2F and 2B versus the spin speed parameter. (b) Variation of the exponential increment parameter 2F versus the spin speed parameter.

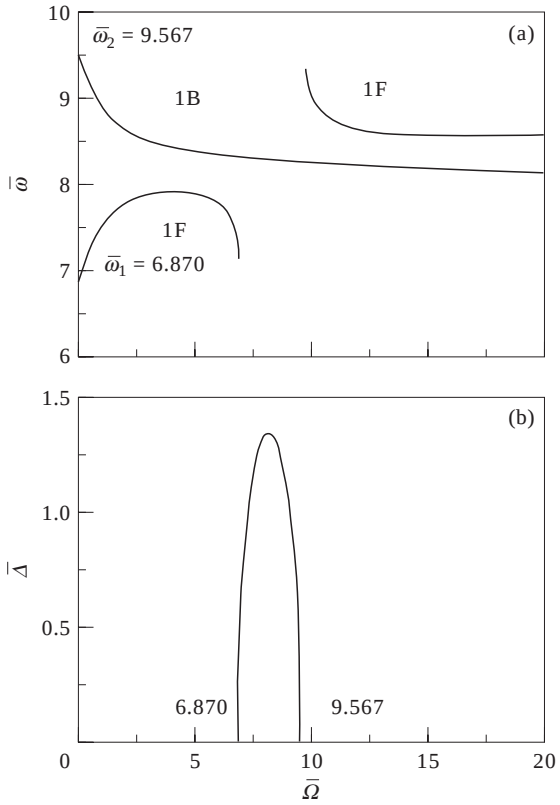

Figure 7.(a) Variation of the whirl speed parameters 1F and 1B versus the spin speed parameter. (b) Variation of the exponential increment parameter 1F versus the spin speed parameter.

Assuming small deformations, the kinetic energy can be linearized and then given by

$$K.E. = T_t + T_r = \frac{1}{2}\int_0^L \{\rho A(\dot{v} - \Omega w)^2 + \rho A(\dot{w} + \Omega v)^2 + \rho I_y\,(\dot{\alpha} - \Omega\beta)^2$$

$$+ \rho I_z\,(\dot{\beta} + \Omega\alpha)^2 + \rho J_p\,(\dot{\phi}^2 + 2\Omega\dot{\alpha}\beta + \Omega^2)\}\,\mathrm{d}x \tag{8}$$

2.2. STRAIN ENERGY

From observation of Figure 4, v and w are the translations of the centerline of the shaft in the y and z directions, and (η, ζ) is the position described by the moving frame. Thus the displacement field can be linearized as

$$u_x = \eta\beta + \zeta\alpha, \qquad u_y = v - \zeta\phi, \qquad u_z = w + \eta\phi. \tag{9}$$

The strain energy U can then be found as

$$U = \tfrac{1}{2}\int_V (\sigma_{xx}\,\varepsilon_{xx} + 2\tau_{xy}\,\varepsilon_{xy} + 2\tau_{xz}\,\varepsilon_{xz})\,\mathrm{d}V$$

$$= \tfrac{1}{2}\int_0^L \{E(I_y\,\alpha'^2 + I_z\,\beta'^2) + GJ_p\,\phi'^2 + \kappa GA[(v' - \beta)^2 + (w' + \alpha)^2]\}\,\mathrm{d}x. \tag{10}$$

2.3. POTENTIAL ENERGY DUE TO THE AXIAL LOAD

The stability problems of the rotating shaft subjected to a compressive axial load P are studied here. The work of this load, arising from the deformation of the shaft, is

$$W = \tfrac{1}{2} P \int_0^L (v'^2 + w'^2)\, \mathrm{d}x. \tag{11}$$

2.4. FINITE ELEMENT FORMULATION

In the present finite element model, the generalized co-ordinate at node i has two translations (v_i, w_i), three rotations $(\alpha_i, \beta_i, \phi_i)$ and their derivative terms $(v_i', w_i', \alpha_i', \beta_i', \phi_i')$. Then the displacement field of the element can be approximated as

$$\begin{Bmatrix} v \\ w \\ \alpha \\ \beta \\ \phi \end{Bmatrix} = \begin{bmatrix} v_i & v_i' & v_{i+1} & v_{i+1}' \\ w_i & w_i' & w_{i+1} & w_{i+1}' \\ \alpha_i & \alpha_i' & \alpha_{i+1} & \alpha_{i+1}' \\ \beta_i & \beta_i' & \beta_{i+1} & \beta_{i+1}' \\ \phi_i & \phi_i' & \phi_{i+1} & \phi_{i+1}' \end{bmatrix} \begin{Bmatrix} N_1(\xi) \\ N_2(\xi) \\ N_3(\xi) \\ N_4(\xi) \end{Bmatrix}. \tag{12}$$

Where $N_i(\xi)$, $i = 1, 2, 3, 4$, is the one-dimensional local cubic Hermite polynomial shape function, and their detailed forms are listed in Appendix A. Equation (12) is substituted

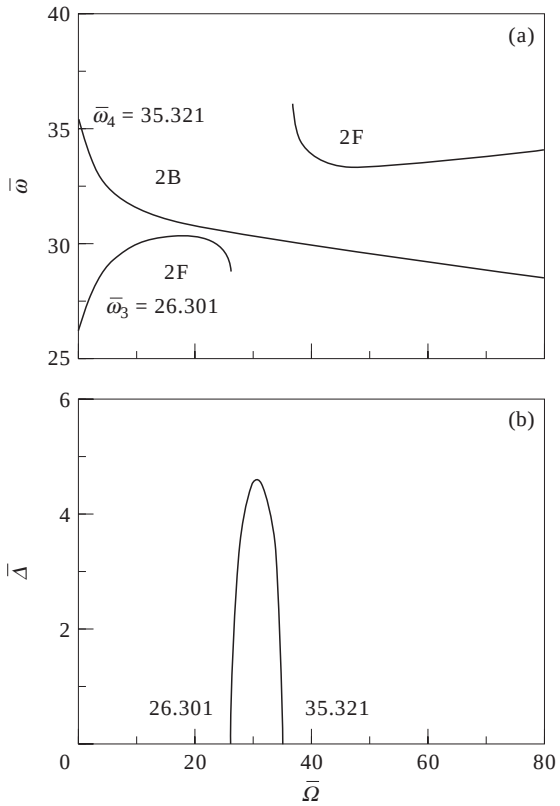

Figure 8.(a) Variation of the whirl speed parameters 2F and 2B versus the spin speed parameter. (b) Variation of the exponential increment parameter 2F versus the spin speed parameter.

TABLE 1

The critical speed parameters of the shaft

Boundary conditions	δ	L/r	$\bar{\omega}_1$	$\bar{\omega}_2$	$\bar{\omega}_3$	$\bar{\omega}_4$
Simply–simply supported	1·0	250	9·867	9·867	39·464	39·464
		25	9·568	9·568	35·322	35·322
	0·4	250	6·242	9·867	24·981	39·464
		25	6·163	9·568	23·789	35·322
Clamped–clamped	1·0	250	22·350	22·350	61·624	61·624
		25	19·910	19·910	48·759	48·759
	0·4	250	14·157	22·350	39·066	61·624
		25	13·458	19·910	35·000	48·759
Clamped–free	1·0	250	3·516	3·516	22·017	22·017
		25	3·464	3·464	20·021	20·021
	0·4	250	2·225	3·516	13·935	22·017
		25	2·210	3·464	13·380	20·021

into equations (8), (10) and (11), and then Hamilton's principle is applied to obtain the governing equations of the complete system:

$$[M]\{\ddot{q}\} + \Omega[G_y]\{\dot{q}\} + ([K] - \Omega^2[K_R] - P[K_G])\{q\} = 0, \tag{13}$$

where $\{q\} = \{v_1, v_1', w_1, w_1', \ldots, \alpha_N, \alpha_N', \beta_N, \beta_N', \phi_N, \phi_N'\}^{\mathrm{T}}$ is the global nodal co-ordinates vector. In order to evaluate the whirl speed of the rotor system, equation (13) is written in the first order state vector form as

$$[A]\{\dot{h}\} + [B]\{h\} = \{0\}, \tag{14}$$

where

$$\{h\} = \begin{Bmatrix} \{\dot{q}\} \\ \{q\} \end{Bmatrix}, \qquad [A] = \begin{bmatrix} [0] & [M] \\ [M] & \Omega[G_y] \end{bmatrix}, \qquad [B] = \begin{bmatrix} -[M] & [0] \\ [0] & [K] - \Omega^2[K_R] - P[K_G] \end{bmatrix}. \tag{15}$$

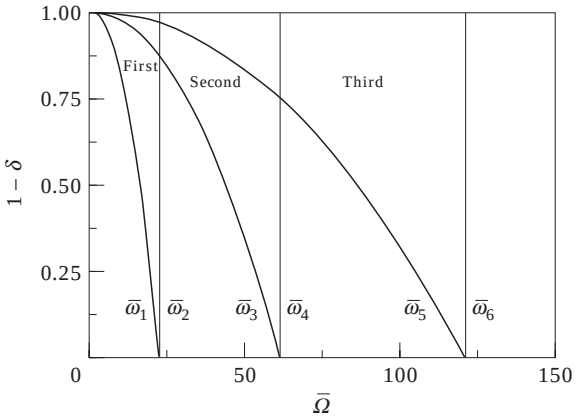

Figure 9. Critical spin speeds versus stiffness ratio.

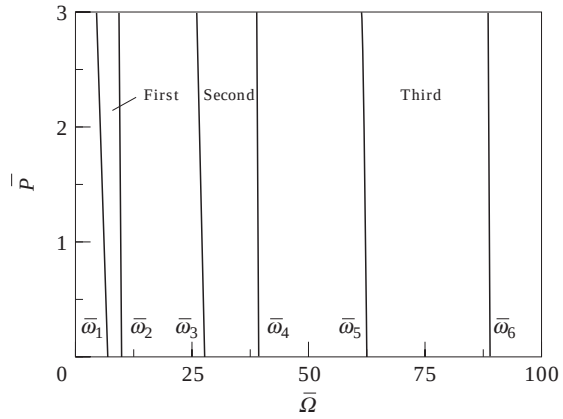

Figure 10. Critical spin speeds versus axial load parameter.

The associated eigenvalue problem of equation (15) is sought from an assumed solution form as

$$\{h\} = \{h_0\}\, e^{\lambda t}, \tag{16}$$

where $\lambda = \Delta + i\theta$, Δ being the real part and θ the natural whirl speed in the rotating frame. The natural whirl speed in fixed frame can be expressed as

$$\omega = \theta \pm \Omega, \tag{17}$$

where "+" is for the forward whirl speed and "−" is for the backward one. When the real part of the eigenvalue λ is greater than zero, the system is unstable.

3. NUMERICAL RESULTS AND DISCUSSION

In this section, the stability of a shaft with dissimilar lateral moments of inertia is studied. To obtain numerical results, the following shaft non-dimensional parameters are adopted throughout: $\delta = EI_z/EI_y$ (stiffness ratio), $\bar{\omega} = \omega(\rho AL^4/EI_y)^{1/2}$ (whirl speed parameter), $\bar{\Omega} = \Omega(\rho AL^4/EI_y)^{1/2}$ (spin speed parameter), $\bar{\Delta} = \Delta(\rho AL^4/EI_y)^{1/2}$ (exponential increment parameter), $\bar{P} = P(L^2/EI_y)$ (axial force parameter).

The frequencies of backward whirling are generally lower than those of forward whirling of the shaft; however, a different phenomenon is observed in this rotor system with dissimilar stiffnesses at low spin speeds. The dependencies of the whirl speeds on the spin speed were calculated for simply supported ends and different slender ratios (L/r, $r = (I_y/A)^{1/2}$). Figures 5 and 6 are for the cases of slenderness ratio = 250 and $\delta = 0{\cdot}5$. If the spin speed is zero, the two natural frequencies $\bar{\omega}_1$ and $\bar{\omega}_2$ are different for the dissimilar stiffnesses in the two principal directions of the shaft, as shown in Figure 5(a). With the spin speed increasing, the backward whirling speeds decrease and the forward ones firstly increase and then decrease suddenly. The first forward whirling speed (1F) is equal to the value zero when the spin speed is equal to 6·987 ($\bar{\omega}_1$); then an instability region of divergent type occurs until the spin speed is larger than 9·867 ($\bar{\omega}_2$). The associated exponential increment parameters, illustrated in Figure 5(b), become positive. Very similar results are obtained for the second mode illustrated in Figure 6. The instability zone is the interval between the spin speeds 27·925 ($\bar{\omega}_3$) and 39·464 ($\bar{\omega}_4$). Obviously, the first instability region is found to be the zone between the spin speeds $\bar{\omega}_1$ and $\bar{\omega}_2$, and the second instability region between the speeds $\bar{\omega}_3$ and $\bar{\omega}_4$.

Here the spin speeds $\bar{\omega}_1$, $\bar{\omega}_2$, $\bar{\omega}_3$ and $\bar{\omega}_4$ are the natural frequencies of the non-rotating shaft indicated in Figures 5(a) and 6(a). Figures 7 and 8 are the whiling speeds for the case of a shaft with slenderness ratio = 25 and $\delta = 0{\cdot}5$. The results show that the first instability zone is between the spin speeds $\bar{\omega}_1$ and $\bar{\omega}_2$, and the second is between the speeds $\bar{\omega}_3$ and $\bar{\omega}_4$. Accordingly, these speeds can be called the critical speeds of the rotating shaft. Therefore, for a long or a short shaft, the task of obtaining the regions of instability lies in calculating the speeds $\bar{\omega}_1$, $\bar{\omega}_2$, $\bar{\omega}_3$ and $\bar{\omega}_4$. Predicting the stability of the rotating shaft consequently becomes simple and time-saving.

The critical speed parameters of a spinning shaft with three cases of distinct end conditions are calculated and shown in Table 1. For the first case ($\delta = 1{\cdot}0$, $L/r = 250$, simply–simply supported ends), the critical speeds $\bar{\omega}_1 = \bar{\omega}_2 = 9{\cdot}867$ and $\bar{\omega}_3 = \bar{\omega}_4 = 39{\cdot}464$ are very close to the natural frequencies of the Euler beam (9·87 and 39·5). The boundary conditions for the other two cases are clamped–clamped and clamped–free ends. The critical speeds of these cases are also very near to those natural frequencies of a Euler beam (the first two natural frequencies are 22·4 and 61·7 for a clamped–clamped supported beam, and 3·52 and 22·0 for clamped–free ends). The critical speed parameters $\bar{\omega}_2$ and $\bar{\omega}_4$ are invariable with a decreasing stiffness ratio. Because these two parameters are the first two bending natural frequencies corresponding to the moment of inertia I_y, and the same I_y is used here, the critical speed parameter of a shorter shaft is lower than a longer one due to the non-dimensional speed being used.

As shown in the study by Rao [3], the Euler beam model was used and its results illustrated that the system is unstable when the whirl speed $\bar{\omega}$ is in the region expressed as:

$$\bar{\omega}_1 < \bar{\omega} < \bar{\omega}_2, \qquad \text{where } \bar{\omega}_1 = \sqrt{\delta}\bar{\omega}_2.$$

According to this analysis, we obtain $\bar{\omega}_1 = 6{\cdot}242$ and $\bar{\omega}_2 = 9{\cdot}870$ for $\delta = 0{\cdot}4$ at simply supported end conditions. These results are very close to those of the present model for the case of $L/r = 250$ in Table 1. However, they are very different between the Euler beam and Timoshenko beam models for $L/r = 25$. This is because the shear deformation greatly affects the dynamic behavior of a short shaft.

The influences of the stiffness ratio are investigated on the critical speeds of a rotating shaft with clamped–clamped end conditions and $L/r = 250$. As indicated in Figure 9, decreasing the stiffness ratio is accompanied by reducing the critical speeds and enlarging the unstable regions of the system. It can be seen that the instability region for a higher mode is larger than a lower one for the same case; these results show that the shaft becomes more unstable at high spin speeds. The influences of axial compressive loads on the simply supported shaft for $L/r = 250$ are shown in Figure 10. If the axial compressive loads increase, the critical speeds decrease and the instability regions enlarge; consequently, when the axial compressive loads increase, the rotating shaft becomes more unstable.

4. CONCLUSIONS

The Timoshenko beam theory is used in this study to predict the stability of a rotating shaft with dissimilar lateral moments of inertia. The natural frequencies of the non-rotating shaft in its two principal directions are not equal. As the spin speed increases, the forward whirling speeds of the shaft will diverge. The instability regions are found to be between the two frequencies corresponding to the same mode of the non-rotating shaft. As the difference between the two lateral stiffnesses of the shaft is increased, the instability regions expand. A decrease in the stiffness ratio consequently makes the shaft more unstable. It

is also observed that the width of a higher mode instability region is larger than that of a lower mode one; therefore, the shaft system is more unstable with an increase in the rotating speeds. Increasing the axial compressive loads will decrease the critical speeds and enlarge the zones of instability.

REFERENCES

1. F. M. Dimentberg 1961 *Flexural Vibration of Rotating Shafts*. London: Butterworth.
2. N. F. Riger and J. F. Crofoot 1997 *Vibrations of Rotating Machinery*. *Part I*: *Rotor–Bearing Dynamics*. Clarendon Hills, Illinois: The Vibration Institute.
3. J. S. Rao 1983 *Rotor Dynamics*. New York: John Wiley.
4. J. M. Vance 1988 *Rotordynamics of Turbomachinery*. New York: John Wiley.
5. M. J. Goodwin 1989 *Dynamics of Rotor–Bearing Systems*. London: Unwin Hyman.
6. H. D. Nelson and J. M. McVaugh 1976 *Transactions of the American Society of Mechanical Engineers*, *Journal of Engineering for Industry* **98**, 593–600. The dynamics of rotor–bearing systems using finite elements.
7. H. D. Nelson 1980 *Transactions of the American Society of Mechanical Engineers*, *Journal of Mechanics Design* **102**, 739–803. A finite rotating shaft element using Timoshenko beam theory.
8. L.-W. Chen and D.-M. Ku 1990 *Journal of Sound and Vibration* **143**, 143–151. Dynamic stability analysis of a rotating shaft by the finite element method.
9. R. M. Laurenson 1976 *American Institute of Aeronautics and Astronautics Journal* **14**, 1444–1450. Modal analysis of rotating flexible structure.
10. H. F. Bauer 1980 *Journal of Sound and Vibration* **72**, 177–189. Vibration of a rotating uniform beam, part I: orientation in the axis of rotation.
11. C. P. Filipich, M. J. Maurizi and M. B. Rosales 1987 *Journal of Sound and Vibration* **116**, 475–482. Free vibrations of a spinning uniform beam with ends elastically restrained against rotation.
12. A. Y. T. Leung and T. C. Fung 1988 *Journal of Sound and Vibration* **125**, 523–537. Spinning finite elements.
13. A. D. Dimarogonas and C. A. Papodopoulos 1983 *Journal of Sound and Vibration* **91**, 583–593. Vibration of cracked shaft in bending.
14. L.-W. Chen and H.-K. Chen 1995 *Journal of Sound and Vibration* **188**, 497–513. Stability of a cracked shaft subjected to the end load.
15. D. C. Kammer and A. L. Schlack 1987 *Journal of Applied Mechanics* **54**, 305–310. Effects of non-constant spin rate on the vibration of a rotating beam.
16. H. P. Lee 1996 *Journal of Sound and Vibration* **189**, 161–171. Dynamic stability of spinning beams of unsymmetrical cross-section with distinct end conditions.
17. Y.-G. Jei 1992 *Journal of Sound and Vibration* **152**, 245–262. Modal analysis of continuous asymmetrical rotor–bearing systems.
18. K. R. Collins, R. H. Plaut and J. Wauer 1991 *Transactions of the American Society of Mechanical Engineers*, *Journal of Vibration and Acoustics* **113**, 74–78. Detection of cracks in rotating Timoshenko shafts using axial impulses.
19. A. C. Lee, Y. Kang, K.-L. Tsai and K.-M. Hsiao 1992 *Transactions of the American Society of Mechanical Engineers*, *Journal of Engineering for Industry* **114**, 465–475. Transient analysis of an asymmetric rotor-bearing system during acceleration.
20. Y. Kang, Y.-P. Shin and A.-C. Lee 1992 *Transactions of the American Society of Mechanical Engineers*, **114**, 194–208. Investigation on the steady-state responses of asymmetric rotors.
21. C. A. Papodopoulos and A. D. Dimarogonas 1987 *Journal of Sound and Vibration* **117**, 81–93. Coupled longitudinal and bending vibrations of a rotating shaft with an open crack.
22. C. A. Papodopoulos and A. D. Dimarogonas 1992 *Transactions of the American Society of Mechanical Engineers*, *Journal of Vibration and Acoustics* **114**, 461–467. Coupled vibration of cracked shafts.
23. S. H. Choi, C. Pierre and A. G. Ulsoy 1992 *Transactions of the American Society of Mechanical Engineers*, *Journal of Vibration and Acoustics* **114**, 249–259. Consistent modeling of rotating Timoshenko shafts subject to axial loads.

APPENDIX A

The cubic Hermite polynomial shape functions:

$$N_1(\xi) = (2 - 3\xi + \xi^3)/4,$$

$$N_2(\xi) = (1 - \xi - \xi^2 + \xi^3)/4,$$

$$N_3(\xi) = (2 + 3\xi - \xi^3)/4,$$

$$N_4(\xi) = (-1 - \xi + \xi^2 + \xi^3)/4.$$

APPENDIX B

The element matrices in equation (13) are:

$$[M] = \begin{bmatrix} [A_{ij}] & 0 & 0 & 0 & 0 \\ 0 & [A_{ij}] & 0 & 0 & 0 \\ 0 & 0 & [B_{ij}] & 0 & 0 \\ 0 & 0 & 0 & [C_{ij}] & 0 \\ 0 & 0 & 0 & 0 & [D_{ij}] \end{bmatrix}_{20 \times 20},$$

$$[G_Y] = \begin{bmatrix} 0 & -2[A_{ij}] & 0 & 0 & 0 \\ 2[A_{ij}] & 0 & 0 & 0 & 0 \\ 0 & 0 & 0 & 0 & 0 \\ 0 & 0 & 0 & 0 & 0 \\ 0 & 0 & 0 & 0 & 0 \end{bmatrix}_{20 \times 20},$$

$$[K] = \begin{bmatrix} [E_{ij}] & 0 & 0 & [J_{ij}] & 0 \\ 0 & [E_{ij}] & [H_{ij}] & 0 & 0 \\ 0 & [I_{ij}] & [F_{ij}] & 0 & 0 \\ [K_{ij}] & 0 & 0 & [G_{ij}] & 0 \\ 0 & 0 & 0 & 0 & [L_{ij}] \end{bmatrix}_{20 \times 20},$$

$$[K_R] = \begin{bmatrix} [\mathrm{A_{ij}}] & 0 & 0 & 0 & 0 \\ 0 & [A_{ij}] & 0 & 0 & 0 \\ 0 & 0 & [C_{ij}] & 0 & 0 \\ 0 & 0 & 0 & [B_{ij}] & 0 \\ 0 & 0 & 0 & 0 & 0 \end{bmatrix}_{20 \times 20},$$

$$[K_G] = \begin{bmatrix} [L_{ij}] & 0 & 0 & 0 & 0 \\ 0 & [L_{ij}] & 0 & 0 & 0 \\ 0 & 0 & 0 & 0 & 0 \\ 0 & 0 & 0 & 0 & 0 \\ 0 & 0 & 0 & 0 & 0 \end{bmatrix}_{20 \times 20},$$

$$[A_{ij}] = \int \rho A N_i N_j \, \mathrm{d}x, \qquad [B_{ij}] = \int \rho I_y N_i N_j \, \mathrm{d}x, \qquad [C_{ij}] = \int \rho I_z N_i N_j \, \mathrm{d}x,$$

$$[D_{ij}] = \int \rho J_p N_i N_j \, \mathrm{d}x, \qquad [E_{ij}] = \int \kappa G A N_i' N_j' \, \mathrm{d}x, \qquad [F_{ij}]$$

$$= \int [EI_y N_i' N_j' + \kappa G A N_i N_j] \, \mathrm{d}x,$$

$$[G_{ij}] = \int [EI_z N_i' N_j' + \kappa G A N_i N_j] \, \mathrm{d}x,$$

$$[H_{ij}] = \int \kappa G A N_i' N_j \, \mathrm{d}x, \qquad [I_{ij}] = \int \kappa G A N_i N_j' \, \mathrm{d}x,$$

$$[J_{ij}] = \int -\kappa G A N_i' N_j \, \mathrm{d}x,$$

$$[K_{ij}] = \int -\kappa G A N_i N_j' \, \mathrm{d}x, \qquad [L_{ij}] = \int G J_p N_i' N_j' \, \mathrm{d}x,$$

$$[M_{ij}] = \int N_i' N_j' \, \mathrm{d}x, \qquad i, j = 1, 2, 3, 4.$$

APPENDIX C: NOMENCLATURE

A	cross-sectional area of shaft section
E, G	Young's and shear modules of the shaft
$[G_Y]$	Gyroscopic matrix
$\vec{i}, \vec{j}, \vec{k}$	unit vector of $oxyz$ frame
I_y, I_z	moments of inertia of the shaft for t_2 and t_3 directions
$[K], [K_G]$	stiffness and geometric matrices
$[K_R]$	stiffness due to the kinetic energy
L	length of the shaft
$[M]$	assembled mass matrix
n	number of independent co-ordinates
N	number of nodes
$N_i(\xi)$	one-dimensional local cubic Hermite polynomial shape function
P	axial compressive load
$\bar{P}$	axial load parameter
$\{q\}$	global displacements vector described in the spin frame $(x \ -y \ -z)$
t_1, t_2, t_3	moving reference frame
T_r	rotational kinetic energy
T_t	translational kinetic energy
u_x, u_y, u_z	displacements of the shaft in the x, y and z directions.
U	strain energy
v, w	translations in the y and z directions
x, y, z	rotating reference frame
X, Y, Z	fixed reference frame
W	work done by axial load
α, β, ϕ	rotations about y-, z- and x-axes, respectively

δ	stiffness ratio
ε_{xx}	normal strain component
ε_{xy}, ε_{xz}	shear strain component
κ	shear correction factor
ξ	local co-ordinate of the element
ρ	mass density of the shaft material
σ_{xx}	normal stress component
τ_{xy}, τ_{xz}	shearing stress component
Ω	spin speed
ω	whirl speed
$\bar{\omega}$	critical speed parameter

Superscripts

T	transpose
$\cdot$	differentiation with respect to time t
$'$	differentiation with respect to x